Journal of Electroceramics, 13, 331–337, 2004


# $SrTiO_3$ Based Side Gate Field Effect Transistor Realized by Submicron Scale AFM Induced Local Chemical Reactions

L. PELLEGRINO,[1,*] E. BELLINGERI,[1] I. PALLECCHI,[1] A.S. SIRI,[1] D. MARRÉ[1] & A. CHINCARINI[2]
[1]*INFM-Lamia, CNR-IMEM, and Dipartimento di Fisica, Università di Genova, via Dodecaneso 33, 16146 Genova, Italy*
[2]*INFN-Genova, via Dodecaneso 33, 16146 Genova, Italy*

Submitted June 25, 2003; Revised October 2, 2003; Accepted July 27, 2004

**Abstract.** In this work we will show how it is possible to apply the so called nano-oxidation technique to pattern electrical circuits on oxygen deficient $SrTiO_3$ (STO) thin films. We will focus on two aspects: the chemical reactions which are triggered at the surface of oxygen deficient STO thin films by the voltage biased tip of an atomic force microscope (AFM) and the exploitation of this phenomenology to pattern insulating regions on oxygen deficient STO thin films in the submicron regime. Due to the insulating nature of the AFM modified regions and to the possibility to remove selectively the modified parts, planar electrical circuits entirely designed over STO thin films can be fabricated. A prototype of planar side gate field effect thin film transistor in which STO acts both as active channel and as gate electrode is presented and discussed.

**Keywords:** atomic force microscope patterning, strontium titanate, field effect, side gate

## Introduction

Perovskite oxides (chemical formula $ABO_3$, A and B cations) represent an intriguing family of compounds in the world of electroceramics. Their physical properties involve a wide range of phenomena such as superconductivity in copper oxides and bismuth oxides [1], ferroelectricity and high-K tunable materials in titanates [2], colossal magnetoresistance in manganites [3] and correlated metallic behavior in ruthenium oxides [4]. Inside each specific phenomenological class, the physical properties depend deeply on the microstructure of the samples (i.e. grain boundaries) and on chemical substitutions which, due to the substitutions sustainable by perovskites, allow to explore a wide range of phase diagrams.

Heterovalent and isovalent chemical substitutions on the cation A and B sites allow to change both the position of the Fermi level into the system and the overlapping among atomic orbitals of the transition metal atoms. These two quantities are mainly involved in the physics of these systems, triggering the appearance of metal-insulator transitions, magnetic and charge ordering etc. [5]...

As a particular example of chemical doping, oxygen stoichiometry is an internal parameter which directly affect the conducting behavior of these oxides. For instance, YBCO superconducting behavior is strongly dependent on oxygen vacancies concentration or oxygen annealing procedure [6]. One of the most widely investigated materials in the class of perovskites is strontium titanate (STO). In its stoichiometric state STO is a high gap insulator with a high dielectric permittivity of about 300 [7] which increases at low temperature to a value of about 10000 at the onset of a quantum state called "quantum paraelectric state" [8]. Isovalent substitutions as Ba on Sr site cause the appearance of a ferroelectric state whose transition temperature depends on the barium concentration [2].

If oxygen vacancies or heterovalent cation substitutions (such as $(La,Sr)TiO_3$, $Sr(Ti,Nb)O_3$) are introduced into STO, a metal-insulator transition onsets. The number of carriers needed to observe a change in the electrical behavior is quite low ($10^{18}$ e/cm) [9] which due to low free electron optical absorption makes

*To whom all correspondence should be addressed. E-mail: pellegri@fisica.unige.it

this material a good candidate as a transparent semiconductor [10]. The low electron density for the appearance of the metal-insulator transition encouraged to use STO as active element in field effect heterostructures where electric charge is induced by an external electric field or by a ferroelectric overlayer [11]. In this respect, a fully STO based device consisting of conducting regions alternated to insulating ones can be envisaged. Because the amount of the oxygen vacancies in STO is thermodynamically related to external oxygen pressure and sample temperature, the growth of alternately stacked stoichiometric and oxygen deficient layers is not possible and the aforementioned all STO devices can be realized only by means of electrochemical reactions after the growth [12].

Concerning a single thin reduced STO film, it would be interesting, at least from a fundamental point of view, to locally modulate the oxygen stoichiometry and study the effects of insulating stoichiometric regions embedded in a conducting reduced STO matrix.

Local oxidation by Atomic Force Microscopy (AFM) o Scanning Tunneling Microscopy at surface of silicon and on thin metal films such as titanium, has been reported by several group in the last years [13]. In these cases, local electrochemical reactions consisting of a simple oxidation of the metal films triggered by the electric field around the AFM tip apex seems to be the main explanation of the observed surface swelling and insulating behavior of the modified regions. In the case of perovskites complicated phenomena at surface are expected due to the number of spurious phases which may appear [14].

In this paper we will present results concerning the idea to perform local electrochemical reactions by an AFM onto conducting STO thin films and reach a local control of the electrical properties of STO. This local control will be exploited to design simple electrical circuits on oxygen deficient STO samples.

## Experimental

Conducting oxygen reduced $SrTiO_3$ thin films are deposited by Pulsed Laser Deposition on insulating $LaAlO_3$ substrates (100) using single STO crystals as target. Substrate temperature during deposition is set in the range 900–1000 K, while oxygen pressure in maintained below $10^{-7}$ mbar. A laser fluency of about 2 J/cm$^2$ with a 3 Hz pulse repetition rate is used. Structural quality of the samples is checked both by an in situ RHEED analysis and by X-ray diffraction. X-ray diffraction measurements in $\theta$–$2\theta$ and $\phi$ scan configurations show epitaxial growth. AFM morphology on as-grown films reveal atomically flat surfaces. Film thickness is measured and calibrated both with X-ray reflectometry, finite size effect and spectroscopic ellipsometry.

Electrical resistivity of the patterned samples is in the 0.01–0.1 Ohm cm range. While thin $SrTiO_{3-\delta}$ films 10–15 nm thick are semiconducting, thicker samples show a slightly metallic behavior and a metal-insulator transition at low temperature which shifts towards high temperature with the decreasing thickness of the film. This fact is probably related to heteroepitaxial stress or to oxygen incorporation from the substrate of the first STO layers which diminishes the number of carriers inside the film.

AFM experiments and imaging were performed with a Park Scientific Microscope in contact mode using conducting $W_2C$ coated silicon tip. Air humidity is varied by controlling an air flux which bubbles into de-ionized water.

To study the effect of the biased AFM tip on the electrical properties of STO, we patterned by standard optical lithography as-grown films in order to obtain 20 $\mu$m wide conducting channels of 15–20 nm thickness which allow for four probes resistance measurements during AFM operations (see Fig. 1). The etching of STO was performed by a HF 10% solution for several seconds in ultrasonic bath. The etching stops at the

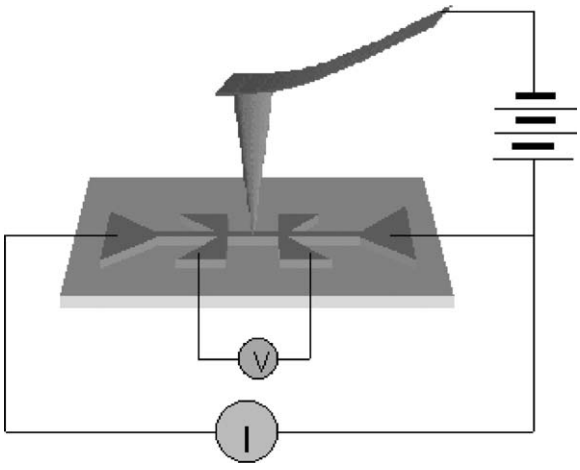


*Fig. 1.* Simple sketch of the apparatus for real time monitoring of the channel resistance during the AFM patterning.

substrate, being $LaAlO_3$ inert to HF chemical attack, and the thickness of the film can be easily confirmed by AFM imaging.

## Results and Discussions

Upon application of a low (1–5 V) negative voltage while scanning the biased tip back and forth transversely along the channel in a dry air, no change in the electrical conductivity and morphology of the channel is observed. By increasing air humidity and applied voltage over a defined threshold a change in channel resistivity appears and, if the voltage is high enough, the vanishing of the current along the channel is observed [15]. AFM imaging of the channel after these operations indicate the appearance of a surface overgrowth in the regions subjected to the tip field.

Since these modifications are induced by the AFM tip, this process can be controlled locally over the film surface as reported in Fig. 2(a).

Statistics done by performing scan lines in different conditions reveal that the height of the surface overgrowth increases with increasing applied voltage [15] to a limit value which is nearly equal to the film thickness. On the other end the efficiency of the growth and the width of the lines depends deeply on air humidity [16]. So far, we achieved by this technique a resolution of about 100 nm obtained in low humidity.

Field induced reactions in perovskite type compounds have been also observed in YBCO where a water mediated electrochemical decomposition in the field of an STM microscope has been reported [17].

Concerning the structural and chemical nature of the modified regions, contact mode imaging on AFM modified 30 × 30 $\mu$m square pads fabricated in high humidity show an increased roughness (2.3 nm) and a granular structure with respect to atomically flat as grown films (Fig. 3).

By stirring the AFM patterns in ultrasonic bath of HCl solution, the overgrowth disappear leaving corresponding grooves inside the film, while the STO film in only slightly etched (1–2 nm of STO film). These grooves extend beneath the surface to an amount which is approximately the 70–100% of the preexisting lines height, indicating that the reactions took place inside the film and not only at the film surface. Therefore by this technique it is possible to realize a voltage dependent etching of the film (see Fig. 2(b)).

If the wet etching process is not performed in ultrasonic bath, grains of the modified part are found over the surface, meaning that probably the modified regions are mainly made of compounds which are not etched in HCl, such as $TiO_2$ or even $SrTiO_3$ grains and are rather mechanically removed by the ultrasonic bath.

In order to investigate the chemical elements involved in these reactions, we performed EDX and XPS analysis on the modified regions. Within the

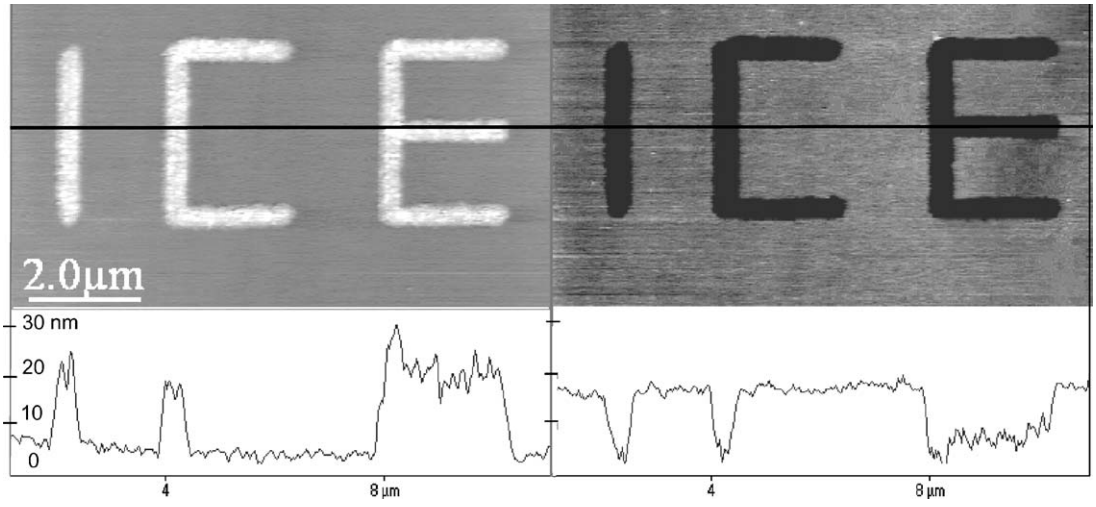


*Fig. 2*. An example of local chemical reactions induced by the negative voltage biased AFM tip before (a) and after the chemical etching (b). The etching removes the chemically reacted outgrowths leaving grooves whose depth is equal or slightly lower than the outgrowth height, meaning that the chemical transformations penetrate into the film.

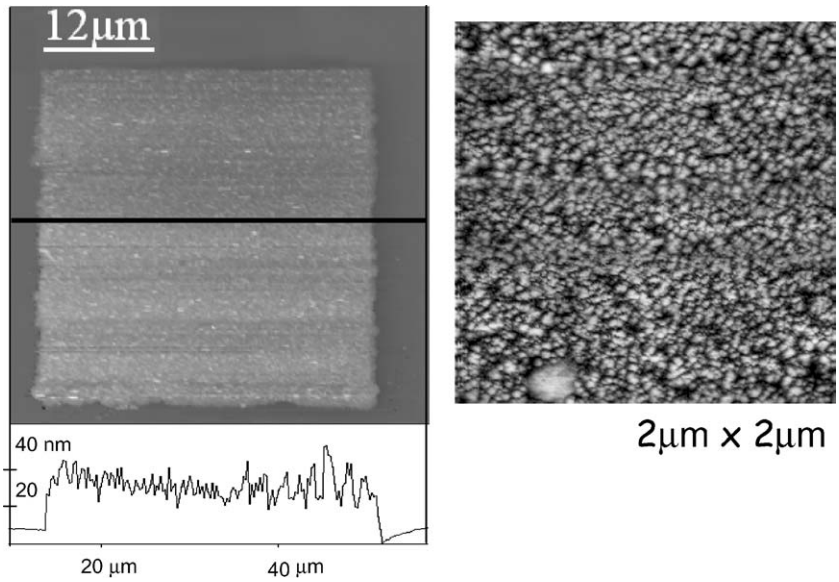


*Fig. 3*. AFM image of a 30 $\mu$m square pattern produced by local oxidation (a) and zoom of its surface (b). The roughness of the modified region is about 2 nm (r.m.s.) and the morphology resembles to the one of the high voltage anodized sample of Fig. 4.

sensitivity of these techniques, no difference in composition is visible between modified and as grown regions and no additional elements coming from the tip such as Si, or W are present.

Because such kind of chemical analyses are problematic on such small AFM modified structures, we studied this process also on a macroscopic scale by fabricating an electrochemical cell for anodic oxidation in which one electrode is the reduced STO film itself while the counter electrode is a platinum foil. The two electrode are immersed in a 0.01 M KOH solution so as to allow electrical conduction. Additional contacts bonded to the STO electrode allow to measure the resistivity of the film during the anodic oxidation. Details about the experimental setup and the applications of this technique to the fabrication of an all-oxide device are reported in ref. [12].

Cyclic voltammetry measurements on oxygen reduced $SrTiO_3$ thin films reveal different regimes: up to 0.75 V no current between the electrodes is experimentally detected. Then, the current increases rapidly together with an increasing in the resistivity of the sample, indicating that some reaction inside the film is taking place. Between 1.2 V and 1.6 V the current increases more slowly, while if the voltage between the electrodes exceed 1.6 V another rapid increasing of the current is easily measured and oxygen evolution at the anode is observed. Basically there seems to exist a voltage threshold at the edge of two different physical-chemical reactions. Typical cyclic voltammetry measurements are reported in Fig. 4 together with three AFM images of an as grown film and of two samples anodized in the two different chemical reaction regimes. The sample anodized with voltages below 1.6 V exhibits no differences in the XRD spectrum and in the surface roughness with respect to as grown films except for the electrical conductivity, while in the case of high voltage anodization, AFM morphological measurements of the surface show an increased roughness which resembles the one observed in the AFM modified regions reported in figure 3b. Moreover, X-rays diffraction measurements show a diminishing of the STO peaks on this latter sample even if no additional crystallographic phases are revealed.

XPS studies performed on such samples conclude that no chemical phases such as SrO or $TiO_2$ can be distinguished because of little binding energy differences between these phases and STO and because of the charging of the sample surface which limits the instrument sensitivity. In the case of the high voltage sample a lack in Sr stoichiometry is observed. At this stage, we conclude that while in the case of low voltage macroscopic anodization a pure oxidation

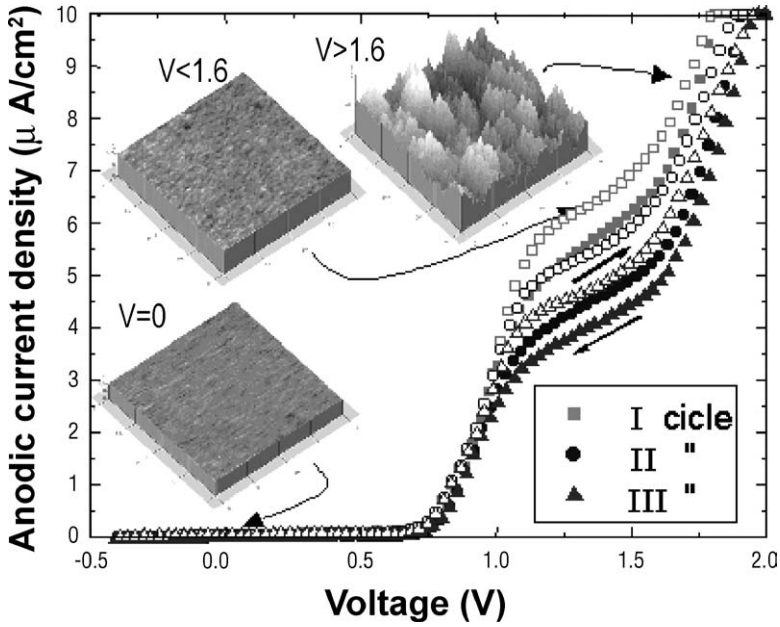


*Fig. 4.* Cyclic voltammetry measurements performed on a conducting STO thin film using the electrochemical cell described in the text. Three different regimes can be distinguished: below 1–1.2 V, where no current flows between the electrodes, between 1.2 and 1.6 V, where the oxidation process takes place and above 1.6 V where the current raises abruptly by increasing the voltage. In this last case the sample structural and morphological properties are completely modified. Three AFM images of samples anodized in the three different regimes are shown in the insets.

of $SrTiO_{3-\delta}$ into $SrTiO_3$ onsets, in the high voltage regime chemical decomposition of STO into SrO, $TiO_2$ and hydroxides takes place. This hypothesis can explain the lack of Sr measured in the high voltage oxidized sample: in this case as the sample is immersed in a water solution, soluble species like $Sr(OH)_2$ dissolves.

We think the reaction induced by the biased tip have the same origin of that which appear in the high voltage regime within the electrochemical cell. Up to now no pure oxidation of $SrTiO_{3-\delta}$ into $SrTiO_3$ has been observed on local experiments, probably due to the large time required to oxidize completely the STO thin film compared to the timescales usually involved in AFM experiments. So far experiments performed in dry air by heating the sample up to 150°C so as to activate oxygen motion show that the increasing of the channel resistance is always correlated to the appearance of the overgrowths.

Modified regions are insulating and if the reactions extends completely down to the substrate electrical insulation can be easily obtained. We studied the insulation properties that can be achieved in a 20 $\mu$m narrow conducting channel by cutting a complete transverse line. Measurements of leakage current of such barriers upon application of voltage sweeps at different temperatures show non linear characteristics with a voltage threshold beyond which the leakage current is no more negligible. This threshold shifts towards high voltages with the decreasing of the temperature. After removing the barrier by wet etching, the insulation improves showing a leakage current below 10 pA with voltage up to 100 V.

While the investigation of the leakage mechanisms is under analysis, we exploited this patterning technique to realize Side Gate Field Effect devices whose active channel and gate pad are made of $SrTiO_{3-\delta}$. An AFM image of typical side gate geometry is reported in the inset of Fig. 5. By this geometry the electric field lines close into the channel from the gate pad through the insulating barrier and the insulating substrate. The amount of induced charge is related to the geometry of the barriers and the dielectric constant of the substrate itself. Previously we reported about the fabrication of such kind of devices showing field effect modulation of the resistance in a STO thin channel, but due to the

low carrier concentration and related high resistance of that channel, low temperature measurements were not possible. A new device was fabricated starting from a slightly thicker film without removing insulating barriers by chemical etching, thus allowing to measure down to 10 K.

In Fig. 5, we report field effect measurements on such a device where the modulation of channel resistance with the same applied voltage clearly increases as the temperature goes down. The maximum change in resistance (R(−40 V) − R(0 V)/R(0 V)) is about 8% obtained by applying 40 V below 30 K. The modulation of the resistance follows approximately a linear behavior with the field at all the temperatures. In all field effect measurements the leakage current was constantly monitored to be negligible with respect to the current used to measure the channel resistance.

The increased field effect modulation at low temperature, more evident in Fig. 6, is not related to changes of the dielectric constant of the substrate, as the $\varepsilon_r$ of $LaAlO_3$ remains approximately constant with temperature [18]. The observed feature can be explained in terms of the decreasing of mobile carrier concentration at low temperature, which results in a major effect of the induced charges on the transport properties of the channel. This hypothesis has been confirmed by Hall effect measurements which show a decreasing of about a factor 3 of the carrier concentration as a function of the temperature from $10^{20}$ $cm^{-3}$ at room temperature to 3 $10^{19}$ $cm^{-3}$ at 50 K. Below 40 K, a plateau in the resistance modulation probably related to a change in the conduction mechanism, is observed.

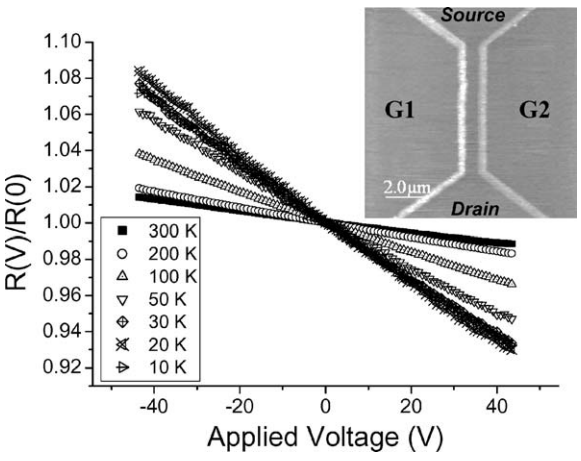


*Fig. 5.* Resistance modulation of the channel of a side gate field effect device as a function of the gate voltage, recorded at different temperatures. (Inset) AFM image of typical side gate geometry.

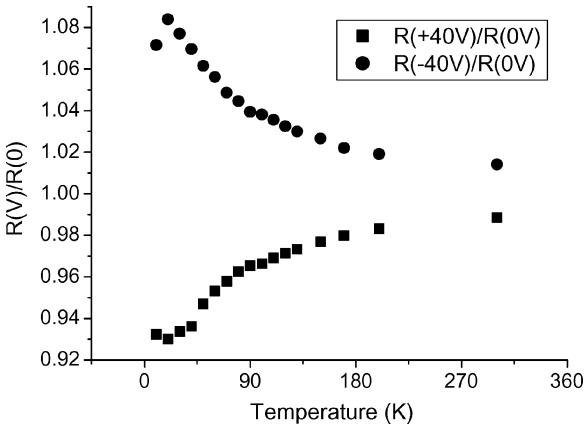


*Fig. 6.* Temperature dependence of the channel resistance modulation upon the application of positive and negative gate voltages. The increasing of the effect can be ascribed to the decreasing of the channel carrier concentration due to the semiconducting behavior of the channel itself.

## Conclusions

Summarizing, we showed that by applying the nano-oxidation technique to thin conducting STO films i.e. by scanning the sample surface by a negative voltage biased AFM tip, a local chemical reaction is induced and insulating regions of sub-micrometric size can be created.

We exploited such result and the possibility of selectively etching the AFM modified regions to pattern electrical circuits on the film surface and realize side gate field effect devices in which resistance modulations up to several percents have been observed. Furthermore, resistance modulation increases by lowering the temperature due to the semiconducting behavior of the channel and show a plateau at low temperature probably related to a change in the conduction mechanism.

More marked changes and in perspective a complete metal-insulator transition are expected by optimizing the device geometry and by using substrates with higher dielectric constant.

## Acknowledgments

This work was done with the financial support of CARIGE foundation. The authors wish to thank Renato Buzio and Daniele Pergolesi for useful discussions. Acknowledgements are also due to Maurizio Canepa for providing the spectroscopic ellipsometer and for discussions.

## References

1. J. Orenstein and A.J. Millis, *Science*, **288**, 468 (2000), B.F. Woodfield,* D.A. Wright, R.A. Fisher, N.E. Phillips, and H.Y. Tang, *Phys. Rev. Lett.*, **29**, 4622 (1999).
2. V.V. Lemanov, E.P. Smirnova, P.P. Syrnikov, and E.A. Tarakanov, *Phys. Rev. B*, **54**, 3151 (1996).
3. S. Jin, T. Tiefel, M. McCormack, R. Ramesh, and L. Chen, *Science*, **264**, 413 (1994).
4. David J. Singh, *J. Appl. Phys.* **79**, 4818 (1996).
5. M. Imada, A. Fujimori, and Y. Tokura, *Metal Insulator Transitions Rev. Mod. Phys.*, **70**(4), (1998).
6. K.-H. Wu, M.-C. Hsieh, S.-P. Chen, S.-C. Chao, J.-Y. Juang, T.-M. Uen, Y.-S. Gou, T.-Yuen Tseng, C.-M. Fu, J.-M. Chen, and R.-G. Liu, *Jpn. J. Appl. Phys.*, Part 1, **37**, 4346 (1998).
7. D. Fuchs, C.W. Schneider, R. Schneider, and H. Rietschel, *J. Appl. Phys.*, **85**, 7362 (1999).
8. K.A. Müller and H. Burkard, *Phys. Rev. B*, **19**, 3593 (1979).
9. O.N. Tufte and P.W. Chapman, *Phys. Rev.*, **155**, 796 (1967).
10. H.H. Wang, F. Chen, S.Y. Dai, T. Zhao, H.B. Lu, D.F. Chui, Y.L. Zhou, Z.H. Chen, and G.Z. Yang, *Appl. Phys. Lett.*, **78**, 1676 (2001).
11. A.G. Schrott, J.A. Misewich, V. Nagarajan, and R. Ramesh, *Appl. Phys. Lett.* **82**, 4770 (2003); D. Marré, A. Tumino, E. Bellingeri, L. Pellegrino, I. Pallecchi, and A.S. Siri, *J. Phys. D: Appl. Phys.*, **36**, 896 (2003); I. Pallecchi, G. Grassano, D. Marré, L. Pellegrino, M. Putti, and A. S. Siri, *Appl. Phys. Lett.*, **78**, 2244 (2001).
12. E. Bellingeri, L. Pellegrino, D. Marré, I. Pallecchi, and A.S. Siri, *J. Appl. Phys.*, **94**, 5976 (2003).
13. J.A. Dagata, J. Schneir, H.H. Harary, C.J. Evans, M.T. Postek, and J. Bennett, *Appl. Phys. Lett.*, **56**, 2001 (1990); E.S. Snow and P.M. Campbell, *Science*, **270**, 1639 (1996).
14. K. Szot and W. Speier, *Phys. Rev. B*, **60**, 5909 (1999).
15. L. Pellegrino, I. Pallecchi, D. Marré, E. Bellingeri, and A.S. Siri, *Appl. Phys. Lett.*, **81**, 3849 (2002).
16. L. Pellegrino, E. Bellingeri, I. Pallecchi, A.S. Siri, and D. Marré, *Solid State Electronics*, **47**, 2193 (2003).
17. G. Bertsche, W. Clauss, and D.P. Kern, *Appl. Phys. Lett.*, **68**, 3632 (1996); G. Bertsche, W. Clauss, F.E. Prins, and D.P. Kern, *J. Vac. Sci. Technol. B*, **16**(6), 3883 (1998).
18. G.A. Samara, *J. Appl. Phys.*, **68**, 4214 (1990).